Available online at www.sciencedirect.com
SCIENCE DIRECT®
Physica D 192 (2004) 196–214
PHYSICA D
www.elsevier.com/locate/physd

Averaged equations for distributed Josephson junction arrays

Matthew Bennett, Kurt Wiesenfeld*

School of Physics, Georgia Institute of Technology, 837 State Street, Atlanta, GA 30332-0430, USA

Received 15 July 2003; accepted 2 January 2004
Communicated by E. Kostelich

Abstract

We use an averaging method to study the dynamics of a transmission line studded by Josephson junctions. The averaged system is used as a springboard for studying experimental strategies which rely on spatial non-uniformity to achieve enhanced synchronization. A reduced model for the near resonant case elucidates in physical terms the key to achieving stable synchronized dynamics.

PACS: 05.45.Xt; 74.81.Fa; 85.25.Pb

Keywords: Josephson junction arrays; Synchronization; Coupled oscillators

1. Introduction

The study of Josephson junction arrays [1,2] is almost as old as the Josephson effect itself [3]. Interest in arrays has remained high due to potential applications in very high frequency electronics [4,5]. In the meantime, beginning with work in the late 1980s, Josephson arrays became a popular class of systems in nonlinear dynamics, serving as an archetype of spontaneous synchronization in coupled oscillator populations [6–10].

Most theoretical work on the nonlinear dynamics of Josephson arrays has been based on lumped circuit descriptions. However, as arrays are pushed to larger numbers of junctions and higher operating frequencies, lumped circuit theories break down. As the wavelength of the emitted radiation becomes smaller than the spatial extent of the array, new physical aspects become important which are ignored in a lumped description. Experimentalists have tried to take advantage of the fact that spatial positioning of the elements is important in the high frequency regime. Han and coworkers [11,12] and Booi and Benz [13] demonstrated that clustering junctions at strategic locations along the wire connecting them can increase the emitted power. This strategy is based on a simple physical picture where the clusters lie at antinodes of a particular standing wave of the (junction-free) wire. One goal of the present paper is to investigate this qualitative picture on a more fundamental, quantitative basis. In the process, we derive equations which can be used to study arbitrary spatial configurations.

* Corresponding author. Tel: +1-404-894-2429; fax: +1-404-894-9958.
E-mail addresses: matthew.bennett@gonzo.physics.gatech.edu (M. Bennett), kurt.wiesenfeld@physics.gatech.edu (K. Wiesenfeld).

0167-2789/$ – see front matter
doi:10.1016/j.physd.2004.01.004

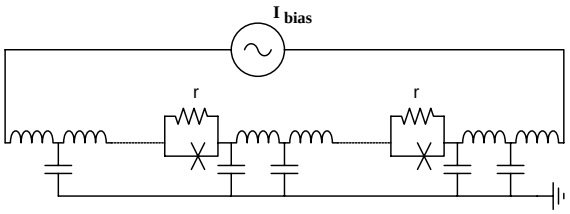

Fig. 1. Schematic of a distributed series array with constant current source I_{bias}. The junctions have resistance r and zero capacitance (the ideal part of a junction is denoted by a cross).

The starting point for our analysis is a model introduced by Cawthorne et al. [14] in which the wire connecting a series array of junctions is treated as a transmission line. As a result, the wire becomes an important dynamical entity; in the lumped (i.e., low-frequency) limit the wire plays no dynamical role whatsoever. In an effort to go beyond numerical simulation, we consider the simplest non-trivial version of the model (see Fig. 1) with no external load so that the junction–junction coupling is entirely due to the transmission line. It is known that this can provide sufficient coupling to induce synchronization in uniform arrays [15].

We apply an averaging scheme [16] to derive a reduced model for the phase dynamics of the junctions. This particular scheme has played a central role in a number of advances in the study of lumped Josephson arrays, in understanding the massive neutral stability of splay phase states [17]; in establishing the connection with the Kuramoto model [18]; and in deriving the frequency matching condition for stability of the inphase state [16].

After deriving the averaged equations, we investigate whether spatially clustered arrays have better synchronization properties than uniform arrays. We find that, when driven near resonance, tightly clustered arrays tend to phase lock better than non-clustered arrays. However, and somewhat surprisingly, we find that increasing the number of junctions within a cluster can diminish synchronization and even wipe it out entirely. Our analysis of a few well-chosen cases leads us to a clear understanding of these effects.

2. Background

A Josephson junction array is traditionally modeled as an electrical circuit and the dynamical evolution equations are derived using Kirchhoff's laws, which represent a low frequency simplification of Maxwell's equations. A schematic of a Josephson array is shown in Fig. 2. N junctions are placed in series and are driven by an externally controlled current I_{bias}; additional elements of the system are modeled as an external load [7,19].

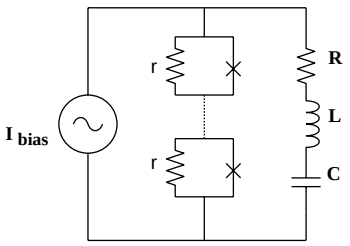

Fig. 2. Schematic of a lumped series array with constant current source I_{bias} and an LRC load. Each junction has resistance r and zero capacitance.

In the Kirchhoff limit, the current in a wire is incompressible: thus, at any instant its value is the same everywhere along its length. The circuit equations for Fig. 2 are

$$\frac{\hbar}{2er}\dot{\phi}_j + I_c \sin\phi_j = I_{\text{bias}} - I_L, \tag{1}$$

$$L\ddot{I}_L + R\dot{I}_L + \frac{1}{C}I_L = \frac{\hbar}{2e}\sum_{k=1}^{N}\ddot{\phi}_k \tag{2}$$

for $j = 1, \ldots, N$, and where ϕ_j is the phase difference of the wavefunction across the jth junction; r and I_c are the junction resistance and critical current, respectively; I_L is the current through the load; L, R, and C are the load parameters; e is the magnitude of the electron charge; and $\hbar$ is Plank's constant divided by 2π. The first equation is a statement of current conservation for each (point) junction. The second equation follows from equating the total voltage drop across the load to that across the array.

The Kirchhoff limit is valid provided that the size of the system is small compared to the wavelength of the electromagnetic radiation. As it happens, the twin technological goals of generating higher operating frequencies ω and larger output powers (and thus more junctions) both work against this limit. This is illustrated in Fig. 3. The oscillator frequency sets the radiation wavelength $\lambda = c/nf$, where c is the speed of light in a vacuum and n is the index of refraction of the wire. Meanwhile, the total length of the system is $l = Nd$, where d is the average spacing between junctions. (The junctions themselves are typically much smaller than d.) To take an example, an array

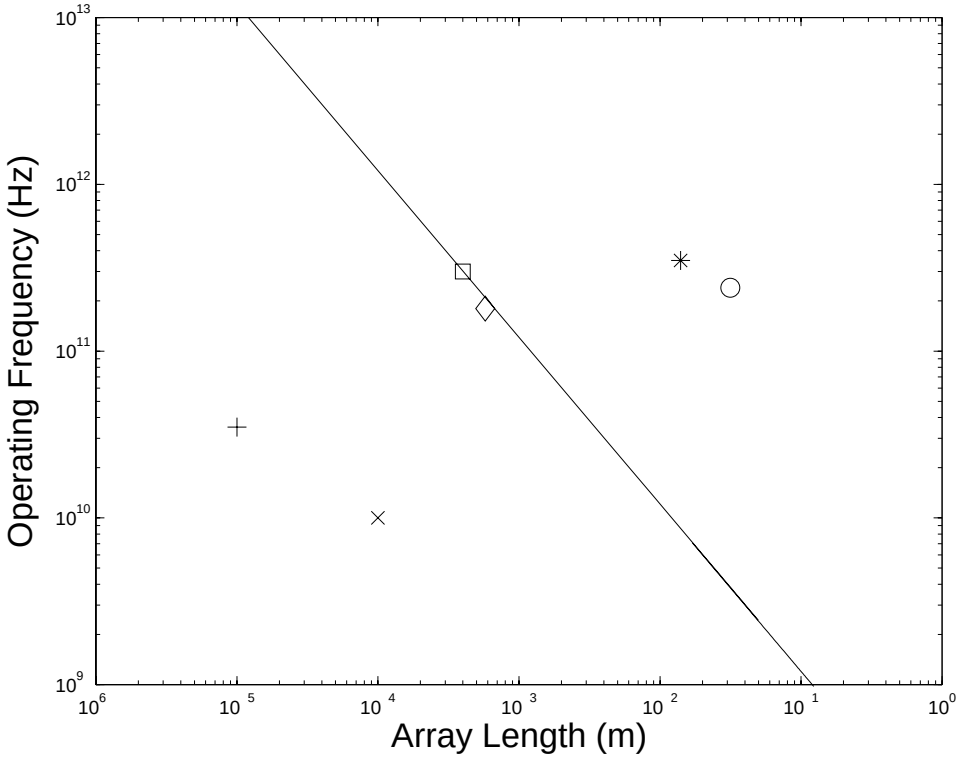

Fig. 3. Curve $f = c/nl$ showing where the radiation wavelength equals the spatial extent of the array (here n is taken to be 2.5, which is typical for Josephson arrays). As the length of the array increases, the frequency regime of the Kirchhoff limit decreases. Also indicated are the points at which some experimental arrays operated ((□) [12]; (○) [13]; (×) [19]; (∗) [20]; (◇) [21]; and (+) [22]).

operating at 300 GHz—not a particularly high frequency for Josephson junctions—corresponds to a wavelength of 0.4 ml when the index of refraction is 2.5; for a typical spacing of 10 μm, this is about the same size as an array of about 40 junctions—not a particularly large number for Josephson arrays.

To date, theorists have paid little attention to the dynamics of Josephson arrays at high frequencies. The problem is more complicated than its low frequency counterpart and in this paper we confine ourselves to the simplest version of the problem, namely where the load is absent. In the Kirchhoff limit, this case is trivial: without a load the junctions are uncoupled and there is no hope of synchronization. But at higher frequencies the current in the wire is not necessarily spatially uniform, so the wire becomes a significant dynamical entity which couples the junctions along its length. Following Ref. [14], we model the wire as a lossless transmission line, so that the governing dynamical equations become

$$\frac{\hbar}{2er}\dot{\phi}_j + I_c \sin\phi_j = I(x_j, t), \quad j = 1, 2, \ldots, N, \tag{3}$$

$$\frac{\partial^2 I}{\partial t^2} - v^2 \frac{\partial^2 I}{\partial x^2} = -\sum_{j=1}^{N} \frac{\hbar}{2eL}\ddot{\phi}_j \delta(x - x_j), \tag{4}$$

where $I(x, t)$ is the wire current at position x and time t; v and L are the wave speed and inductance per unit length of the wire, respectively. The first equation is again the statement of current conservation for each (point) junction. The second is the evolution equation for a lossless transmission line with each junction acting as a spatially localized, time-dependent voltage source. (See Ref. [15] for a simple derivation.)

The boundary conditions are

$$I(0, t) = I(l, t) = I_{\text{bias}},$$

where l is the length of the wire and I_{bias} is the bias current. Experimentally, I_{bias} is the most directly accessible control parameter. It controls the oscillator frequencies: the larger I_{bias} the higher the frequency.

The goal is to have an attracting inphase state, so that the junction voltages (proportional to $\dot{\phi}_j$) all oscillate with the same frequency and phase. It is also desirable that the amplitude of the oscillations be as large as possible. It is debatable whether the inphase state has ever been achieved in any real Josephson junction array; estimates suggest [18] that existing arrays need to use junctions which are matched to within 1 or 2%, which is just barely attainable with existing technology [23].[1] What is certain is that the best reported results for total output power at high frequencies used spatially non-uniform arrays built with a periodic structure. The idea behind the "resonant architecture" used in these experiments is as follows. Imagine that the junctions oscillate at a frequency close to the resonant frequency of one of the normal modes of the transmission line. Then one expects large amplitude response of this particular mode; if the junctions are placed at "equivalent positions" relative to this mode, they will all feel the same (large) ac drive, which presumably is beneficial for generating inphase oscillations. Moreover, one expects the most effective scheme would be to place the junctions at antinodes of the resonant mode.

This picture has a strong physical appeal, but there is little theoretical basis to justify it [24,25]. Naturally, it would be desirable to put the basic idea on a firm quantitative footing (assuming that it is correct). Beyond this, the picture leaves open certain rather important practical questions. For example, to maximize the total power it is desirable to maximize the number of inphase junctions. If one places a group of junctions near each equivalent site, how large (relative to the mode wavelength) can this group be? Similarly, is it acceptable to place junctions (or groups of junctions) at each half-wavelength [12] rather than at each wavelength [11]? It has been argued that

[1] We refer here to arrays of capacitanceless junctions. The situation is predicted to be better for junctions with an optimized capacitance.

although neighboring antinodes represent local current flow of opposite polarity, this is irrelevant for the purposes of synchronization.

3. Derivation of averaged equations

We begin by putting Eqs. (3) and (4) into dimensionless form. We make the following rescalings:

$$t \to \frac{2erI_c}{\hbar}t, \qquad I \to \frac{I}{I_c}, \qquad x \to \frac{x}{l},$$

and introduce spatial Fourier decompositions

$$I(x,t) = I_b + \sum_{k=1}^{\infty} A_k(t)\sin(\pi k x), \qquad \delta(x - x_j) = \sum_{k=1}^{\infty} 2\sin(\pi k x_j)\sin(\pi k x).$$

With these, Eqs. (3) and (4) become

$$\dot{\phi}_j + \sin\phi_j = I_b + \sum_{k=1}^{\infty} a_{jk}A_k, \quad j = 1, 2, \ldots, N, \tag{5}$$

$$\ddot{A}_k + \omega_k^2 A_k = -2\alpha \sum_{j=1}^{N} a_{jk}\ddot{\phi}_j, \quad k = 1, 2, \ldots, N, \tag{6}$$

where the overdot now denotes differentiation with respect to the dimensionless time and

$$\alpha = \frac{\hbar}{2eI_cLl}, \qquad \omega_k = \frac{\pi\hbar k v}{2erlI_c}, \qquad I_b = \frac{I_{\text{bias}}}{I_c}, \qquad a_{jk} = \sin(\pi k x_j).$$

We now follow the averaging procedure of Refs. [16,26]. We first transform the phases ϕ_j into the natural angles ψ_j given by

$$\psi_j(\phi_j) = 2\tan^{-1}\left[\sqrt{\frac{I_b - 1}{I_b + 1}}\tan\left(\frac{\phi_j}{2} + \frac{\pi}{4}\right)\right], \qquad \phi_j(\psi_j) = 2\tan^{-1}\left[\sqrt{\frac{I_b + 1}{I_b - 1}}\tan\left(\frac{\psi_j}{2}\right)\right] - \frac{\pi}{2}.$$

The ψ_j variables are "natural" in the sense that the angular velocities $\dot{\psi}_j$ are constant in the uncoupled limit, whereas the corresponding $\dot{\phi}_j$ are not. Differentiating Eq. (5) and substituting the resulting expression for $\ddot{\phi}$ into Eq. (6) yields

$$\dot{\psi}_j = 1 + \sum_{k=1}^{\infty} \frac{a_{jk}A_k}{I_b - \sin\phi_j}, \tag{7}$$

and

$$\omega^2\ddot{A}_k + \omega_k^2 A_k = -2\alpha \sum_{j=1}^{N} a_{jk}\left\{\sin\phi_j\cos\phi_j - I_b\cos\phi_j + \sum_{l=1}^{\infty} a_{jl}(\omega\dot{A}_l - A_l\cos\phi_j)\right\}, \tag{8}$$

where $\omega = \sqrt{I_b^2 - 1}$ and we have rescaled time once again: $t \to \omega t$.

The sum over l is a significant complication since it couples together all of the modes. Simulations show that one cannot summarily drop these terms. On the other hand, one can show that the relevant contribution of the $A_l\cos\phi_j$

term is expected to be smaller than the $\omega\dot{A}_l$ term by a factor of I_b^2. Our numerical simulations are consistent with this, and we find that neglecting only the $A_l \cos\phi_j$ term yields accurate results. In what follows, we make this (uncontrolled) approximation since it substantially simplifies the ensuing analysis. We also use the trigonometric identities

$$\cos\phi = \frac{\omega \sin\psi}{I_b - \cos\psi} \quad \text{and} \quad \sin\phi = I_b - \frac{I_b^2 - 1}{I_b - \cos\psi} = \frac{1 - I_b \cos\psi}{I_b - \cos\psi} \tag{9}$$

to write

$$\sin\phi_j \cos\phi_j - I_b \cos\phi_j = \frac{C^{(0)}}{2} + \sum_{p=1}^{\infty} (B^{(p)} \sin(p\psi_j) + C^{(p)} \cos(p\psi_j)),$$

where, in particular, $C^{(0)} = C^{(1)} = 0$ and

$$B^{(1)} = 2\omega^2(\omega - I_b). \tag{10}$$

We will see later that in this last sum, only the term involving $\sin\psi$ survives the averaging procedure, so we can safely ignore all terms with $p > 1$. Dropping these, Eq. (8) becomes

$$\omega^2 \ddot{A}_k + \omega_k^2 A_k = -2\alpha \sum_{j=1}^{N} a_{jk} B^{(1)} \sin\psi_j - 2\alpha\omega \sum_{l=1}^{\infty} \sum_{j=1}^{N} a_{jk} a_{jl} \dot{A}_l. \tag{11}$$

The averaging scheme treats the coupling term in Eq. (7) as small, so that in the uncoupled limit $\psi_j(t) = t + \gamma_j$, where γ_j is the initial value of ψ_j. Substituting this into Eq. (11) leads to a steady-state solution

$$A_k = M_k \sin t + N_k \cos t, \tag{12}$$

where the M_k and N_k are determined by the linear system

$$(\omega_k^2 - \omega^2) M_k - \sum_{l=1}^{\infty} \eta_{kl} N_l = f_k, \tag{13}$$

$$(\omega_k^2 - \omega^2) N_k + \sum_{l=1}^{\infty} \eta_{kl} M_l = g_k \tag{14}$$

with

$$f_k = -2\alpha \sum_{j=1}^{N} a_{jk} B^{(1)} \cos(\gamma_j), \qquad g_k = -2\alpha \sum_{j=1}^{N} a_{jk} B^{(1)} \sin(\gamma_j),$$

and

$$\eta_{kl} = 2\alpha\omega \sum_{j=1}^{N} a_{jk} a_{jl}. \tag{15}$$

Solving this linear system (see Appendix A) we can write $A_k(t)$ as

$$A_k = \sum_{j=1}^{N} \{P_{jk} \sin(t + \gamma_j) - Q_{jk} \cos(t + \gamma_j)\}. \tag{16}$$

Substitution of (16) into Eq. (7) and using Eq. (9) yields

$$\dot{\psi}_j = 1 + \sum_{k=1}^{k_{\max}} \frac{1}{\omega^2} a_{jk} A_k(t)(I_b - \cos\psi_j),$$

where $k_{\max}$ is the cutoff value used for k (see Appendix A). We are now ready for the averaging step. We replace ψ_j on the right-hand side with its approximation $\psi_j = t + \gamma_j$ and average the resulting equation over one period:

$$\langle\dot{\psi}_j\rangle = 1 + \frac{1}{2\pi\omega^2} \sum_{k=1}^{k_{\max}} a_{jk} \int_0^{2\pi} A_k(t)(I_b - \cos(t + \gamma_j))\,\mathrm{d}t.$$

This last equation makes it apparent why only the first harmonics of A_k were needed: upon averaging, all higher harmonics integrate to zero.

The final step is to drop the angular brackets and replace the initial values γ_j by the slowly evolving ψ_j. This yields the final averaged equations

$$\dot{\psi}_j = 1 + \frac{1}{2\omega^2} \sum_{i=1}^{N} \sum_{k=1}^{k_{\max}} a_{jk} W_{ik} \sin(\psi_i - \psi_j + \Theta_{ik}), \tag{17}$$

where

$$W_{ik} = \sqrt{P_{ik}^2 + Q_{ik}^2} \quad \text{and} \quad \Theta_{ik} = \tan^{-1}\left(\frac{Q_{ik}}{-P_{ik}}\right).$$

Eq. (17) can be further simplified to

$$\dot{\psi}_j = 1 + \frac{1}{2\omega^2} \sum_{i=1}^{N} M_{ji} \sin(\psi_i - \psi_j + \Omega_{ji}) \tag{18}$$

with

$$M_{ji} = \sqrt{\left(\sum_{k=1}^{k_{\max}} a_{jk} P_{ik}\right)^2 + \left(\sum_{k=1}^{k_{\max}} a_{jk} Q_{ik}\right)^2} \quad \text{and} \quad \Omega_{ji} = \tan^{-1}\left[\frac{\sum_{k=1}^{k_{\max}} a_{jk} Q_{ik}}{-\sum_{k=1}^{k_{\max}} a_{jk} P_{ik}}\right].$$

Eq. (18) is our main result. In form it is very similar to the averaged equation for the loaded lumped circuit problem, Eqs. (1) and (2). When suitably rearranged that equation has the form [26]

$$\dot{\psi}_k = 1 + C \sum_{j=1}^{N} \sin(\psi_j - \psi_k - \delta), \tag{19}$$

where C and δ are constants. Eq. (18) differs from (19) in two ways. First, the coupling constants M_{ji} and phase shifts Ω_{ji} are pair dependent. Second, although one has simple closed form expressions for C and δ, M_{ji} and Ω_{ji} must, in general, be computed numerically by solving the linear system equation (A.1). On the other hand, we have derived Eq. (18) without placing any restrictions on the placement of the junctions, so it is a useful starting point for studying various spatial configurations.

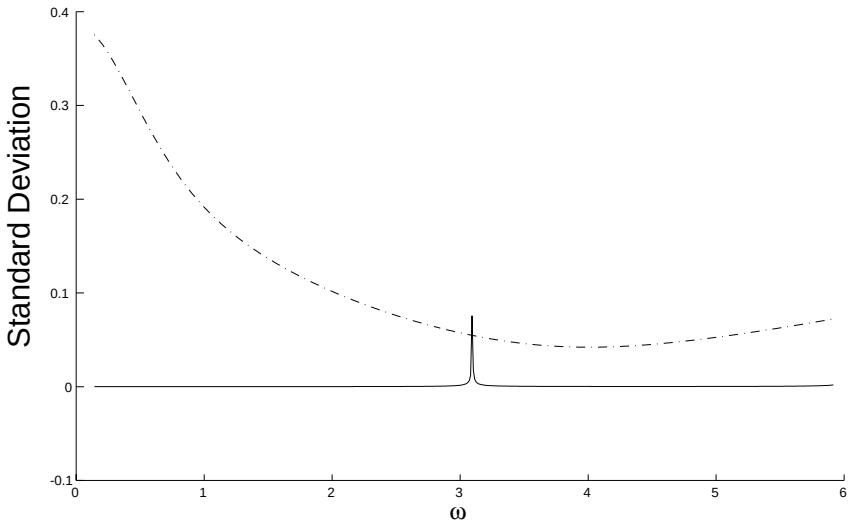

Fig. 4. Normalized standard deviation of $\sum_{i=1}^{N} M_{ji} \sin \Omega_{ji}$ vs. ω. The two curves represent 10 junctions placed evenly along the wire (dash-dot curve); and clustered about the points $x = 1/3$ and $x = 2/3$ (solid curve). A standard deviation near zero represents j-independence of $\sum_{i=1}^{N} M_{ji} \sin \Omega_{ji}$ and hence existence of inphase solutions.

4. Existence and stability of inphase states

In the usual terminology, an inphase state is fully symmetric, i.e., $\phi_j(t) = \phi_1(t)$ for all j. While such solutions always exist for the lumped circuit problem Eqs. (1) and (2), they typically do not exist for the distributed problem Eqs. (3) and (4). The same distinction holds for the corresponding averaged versions, Eqs. (19) and (18), respectively. However, for certain spatial arrangements, the inphase state does exist, namely those for which the combination of system parameters $\sum_{i=1}^{N} M_{ji} \sin \Omega_{ji}$ is independent of j. Note that this condition depends on both the junction positions and the operating frequency. This point is illustrated in Fig. 4. This plot shows the normalized standard deviation of $\sum_{i=1}^{N} M_{ji} \sin \Omega_{ji}$ (as a function of j) versus ω. The dash-dot curve represents a configuration of 10 junctions evenly spaced along the wire. As can be seen, an inphase solution does not exist for any frequency $0 < \omega < 6$. The solid curve represents a configuration in which the 10 junctions have been rearranged such that they are clustered about the points $x = 1/3$ and $x = 2/3$. The standard deviation has nearly gone to zero, so there are inphase solutions except in a small range of operating frequencies near $\omega = 3$.

When the inphase state exists, it is straightforward to check its stability. Setting $\psi_j(t) = \psi_0(t) + \xi_j(t)$, we linearize Eq. (18) for small ξ_j, with the result

$$\dot{\xi}_j = \frac{1}{2\omega^2} \sum_{i=1}^{N} \left[\sum_{k=1}^{k_{\max}} a_{jk} P_{ik} \right] (\xi_j - \xi_i). \tag{20}$$

From here it is an easy matter to solve the linear system equation (A.1) numerically, and hence find the stability matrix for Eq. (20). The eigenvalues of the stability matrix determine the stability of the inphase state. One eigenvalue is constrained to be zero (since the orbit is neutrally stable to perturbations tangent to it); if all other eigenvalues have negative real part then the inphase state is linearly stable.

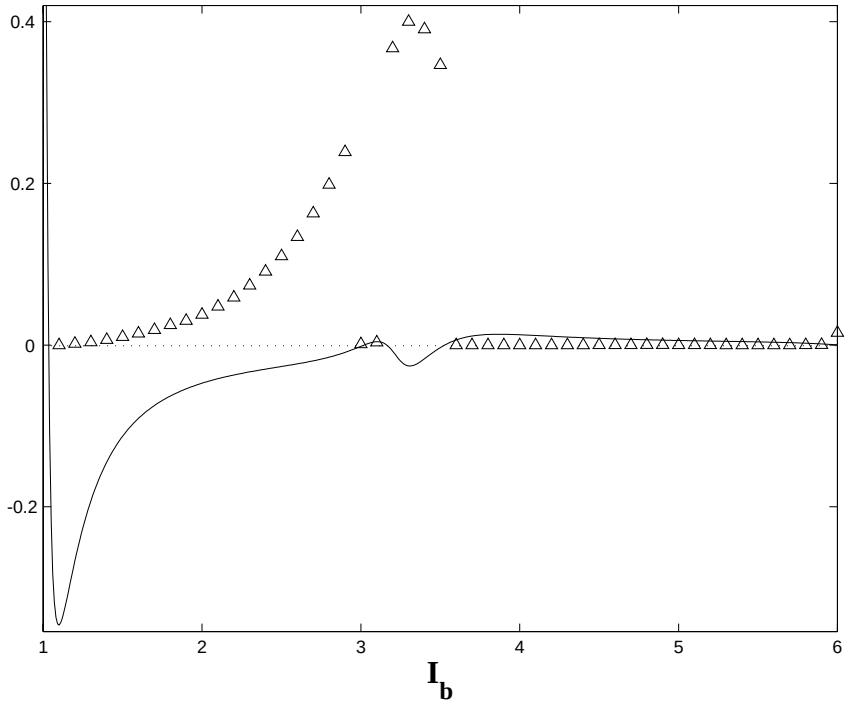

Fig. 5. Plot of the largest non-zero eigenvalue (solid line) of Eq. (20) and the emitted power (triangles) computed by direct integration (arbitrary units). Here there are two junctions at $x_j \in \{1/3, 2/3\}$, $k_{\max} = 15$, $\alpha = 2$ and $v = 1/\pi$.

We have investigated the stability of the inphase state for various array configurations. There is good agreement between the eigenvalue analysis based on the averaged equations and direct numerical simulations of the differential equations (5) and (6), especially when α is of the order of unity or smaller. For larger α, the approximations made in the averaging derivation break down. We assumed that the coupling between the current modes A_k and the junctions ϕ_k was small. From Eq. (6) it is clear that the larger α, the larger A_k; from Eq. (5) we see that this increases the coupling to the junctions, in turn.

Figs. 5 and 6 show plots of the largest non-zero eigenvalue determined from Eq. (20) along with the total emitted power obtained by direct integration of Eqs. (5) and (6). The emitted power is calculated by time averaging the ac part of $\sum_{i=1}^{N} \dot{\phi}_i^2$. Prominent in Fig. 5 is the window around $I_b \approx 3.5$ where the leading eigenvalue dips below zero (indicating stable inphase solutions) and the emitted power is maximized. There is a much wider window of stable inphase states for lower values of I_b; here the emitted power is relatively low because the voltage oscillation amplitude of the individual junctions is small. Above and below the narrow window the emitted power is low because the junction oscillations are incoherent. Fig. 6 shows a similar pattern. The emitted power is low whenever the leading eigenvalue is positive; conversely, the emitted power can be quite large when the inphase state is stable. We show in Fig. 7 examples of the coherence properties of phase locked junctions. Fig. 7(a) shows incoherent behavior, while Fig. 7(b) and (c) show coherent behavior with low and high amplitudes, respectively. The example shown in Fig. 7(b) emits very little power compared to that shown in Fig. 7(c) because of its relatively low amplitude.

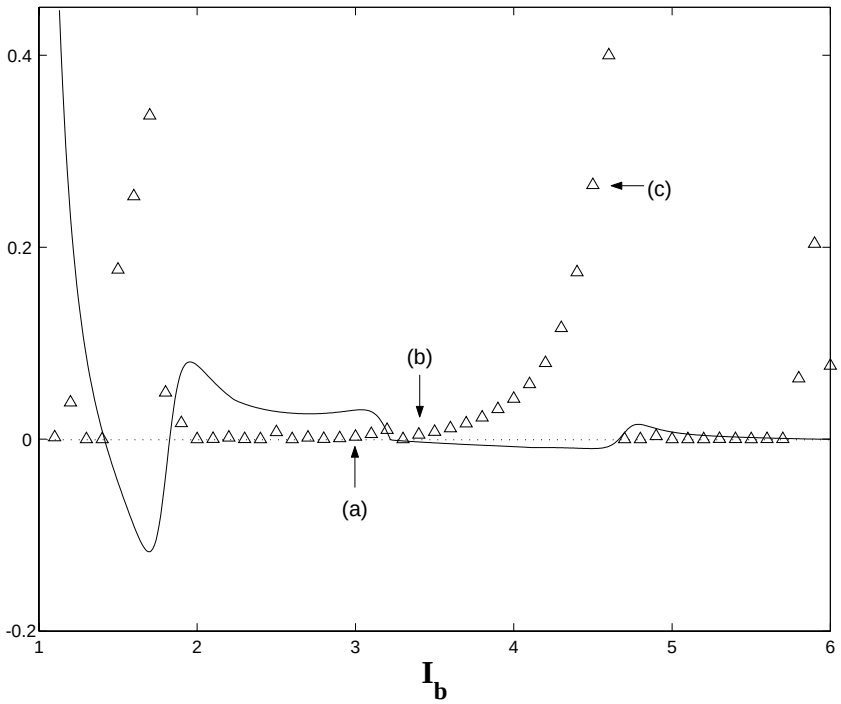

Fig. 6. Plot of the largest non-zero eigenvalue (solid line) of Eq. (20) and the emitted power (triangles) computed by direct integration (arbitrary units). Here there are four junctions, two each at $x_j \in \{1/6, 5/6\}$, $k_{\max} = 15$, $\alpha = 1$ and $v = 1/\pi$. Also shown (arrows) are the three trials plotted in Fig. 7.

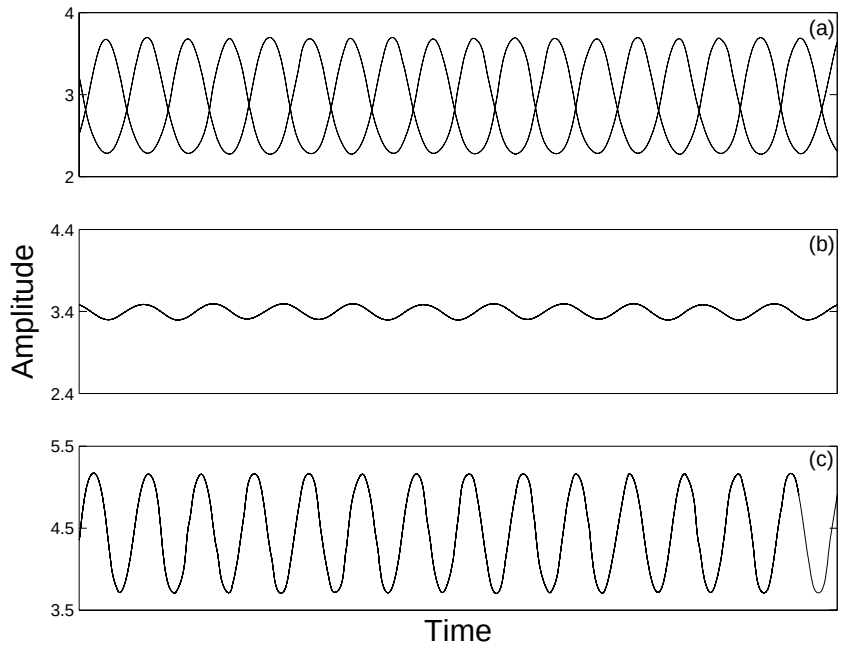

Fig. 7. Comparison of the coherence and amplitude properties of phase locked junctions. Plotted are the three trials indicated in Fig. 6. These trials are examples of (a) incoherent phase locking, (b) low and (c) high amplitude coherent phase locking.

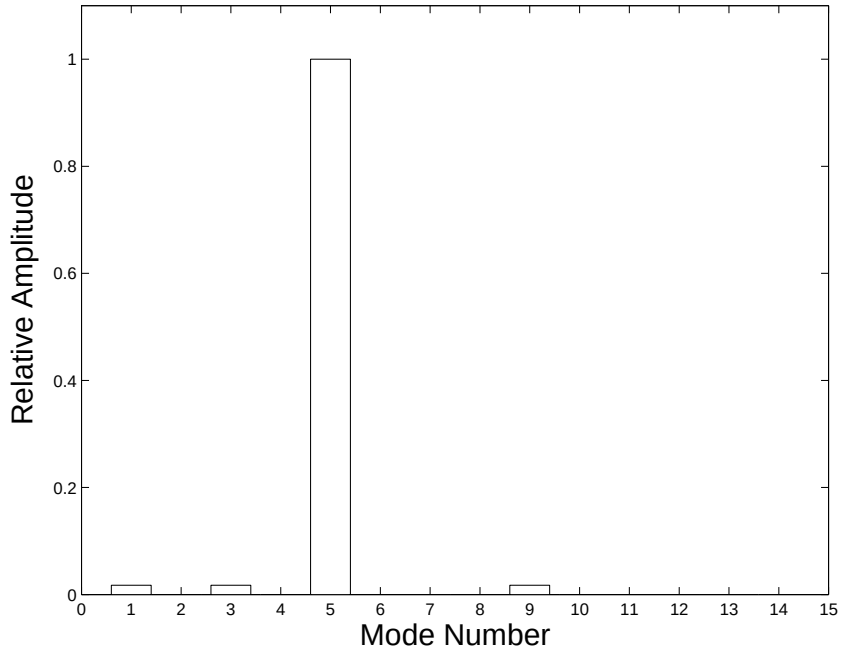

Fig. 8. Histogram of the mode amplitudes (relative to the fifth) of a configuration designed to select the fifth mode. Here there are six junctions at $x_j \in \{1/10 \pm 0.01, 1/2 \pm 0.01, 9/10 \pm 0.01\}$. The bias current was chosen such that $\omega/\omega_5 \approx 1.01$, with $\alpha = 0.01$ and $k_{\max} = 15$.

5. Near resonant behavior

We now take a look at the case of near resonant behavior and the dynamical consequences of spatially clustering the junctions. We take for inspiration experiments [11,13,20] which use arrays intended to operate at a normal mode frequency of the transmission line. (By this we mean the modes in the absence of the junctions, corresponding to a particular Fourier index $k = k^\star$.) Numerically this situation is easily achieved. Fig. 8 is a plot of the mode amplitudes of a configuration designed to select the fifth mode. Clearly the fifth mode is dominant, as is also seen in the RMS current profile shown in Fig. 9. In analytic terms, selecting a particular mode is tantamount to choosing I_b such that $\omega = \sqrt{I_b^2 - 1}$ is very close to ω_5 and choosing a junction configuration that is commensurate with the mode profile.

Let us first see what we can conclude without specifying the junction positions $\{x_i\}$. In the resonant case, we expect the current mode corresponding to $k^\star$ to have a much larger amplitude than the others and hence all sums over k will be dominated by the term involving $k^\star$. Writing $a_j = a_{jk^\star} = \sin(\pi k^\star x_j)$ and keeping just the $k^\star$ term in each sum over the modes, Eq. (18) reduces to

$$\dot{\psi}_j = 1 + K \sum_{i=1}^{N} a_j a_i \sin(\psi_i - \psi_j + \theta), \tag{21}$$

where

$$K = \frac{2\alpha(I_b - \omega)}{\sqrt{(\omega_{k^\star}^2 - \omega^2)^2 + (2\alpha\omega \sum_{q=1}^{N} a_q^2)^2}},$$

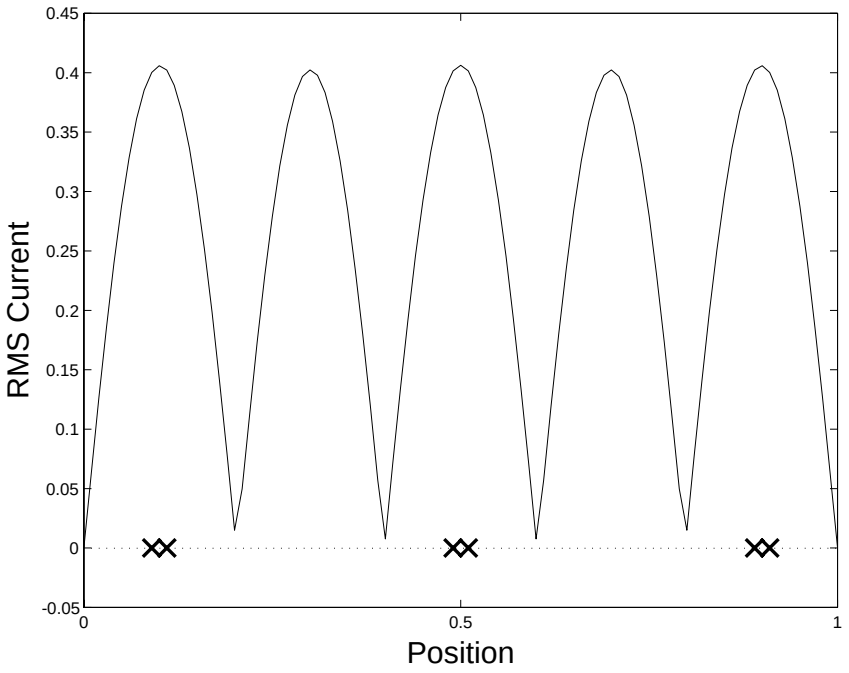

Fig. 9. Plot of the RMS current profile of the example given in Fig. 8. Also shown (crosses) are the positions of the six junctions.

and

$$\theta = \tan^{-1}\left[\frac{2\alpha\omega\sum_{q=1}^{N} a_q^2}{\omega^2 - \omega_{k^\star}^2}\right].$$

Eq. (21) is significantly simpler than Eq. (18). We now have explicit expressions for both the coupling constants and the phase shift. Also, and importantly, the phase shift matrix Ω_{ji} reduces to a constant phase shift θ.

It is still difficult to make analytic progress for arbitrary junction placements, but significant insight can be obtained from examining two simple cases. First consider the case where the junctions are in one "group". By this we mean that the junctions have the property $a_j = a$ for all j. This condition is most obviously met when all of the (pointlike) junctions are at the same spot, but also includes any arrangement where they occupy similar places along the waveform of the mode. In other words, the junctions can be at any position x that satisfies the equation $\sin(\pi k^\star x) = a$ for $x \in [0, 1]$. Fig. 10 illustrates a possible configuration that satisfies this condition.

Wan et al. [20] proposed a design that falls within this category. They used a so-called "quasilumped" circuit which places junctions uniformly along the wire such that the spacing between them was exactly one wavelength of the desired operating frequency. In this manner, each junction is thought to see the same amplitude and phase of the ac current provided that the chosen mode is dominant.

When such a one group situation exists, Eq. (21) becomes

$$\dot{\psi}_j = 1 + a^2 K \sum_{i=1}^{N} \sin(\psi_i - \psi_j + \theta). \tag{22}$$

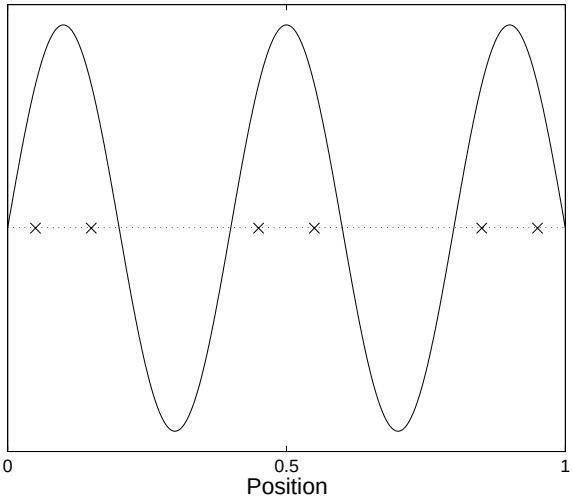

Fig. 10. A configuration of junctions which satisfies the one "group" condition. The junctions are denoted by crosses.

This admits an inphase state $\psi_j = \psi_0$ for all j. Introducing small perturbations $\psi_j = \psi_0 + \xi_j$, the linearized equations are diagonalized by switching to the coordinates $\sigma = \sum_{i=1}^{N} \xi_i$ and $\delta_j = \xi_{j+1} - \xi_j$, with the result:

$$\dot{\sigma} = 0, \tag{23}$$

$$\dot{\delta}_j = -Na^2 K \cos(\theta)\delta_j. \tag{24}$$

So, there is one zero eigenvalue and $N-1$ degenerate eigenvalues given by

$$\lambda = -Na^2 K \cos\theta.$$

Since K is positive the condition for linear stability is then given by

$$\cos\theta = \frac{\omega^2 - \omega_{k^\star}^2}{\sqrt{(\omega_{k^\star}^2 - \omega^2)^2 + (2\alpha\omega Na^2)^2}} > 0$$

or, rather,

$$\omega > \omega_{k^\star}. \tag{25}$$

This result is nearly identical to the one for the RLC-loaded array studied in the lumped limit [19,26]. There, the condition for inphase stability is $\omega > \omega_0$, where $\omega = \sqrt{I_b^2 - 1}$ and ω_0 is the natural frequency of the RLC load. We see that the mode frequency $\omega_{k^\star}$ in the transmission line model (without load) plays the role of the load frequency ω_0 in the lumped model.

As a second example, consider the case of two groups. By this we mean that there are $n_1 + n_2 = N$ junctions such that n_1 junctions have the property $a_{jk^\star} = a_1$ and n_2 junctions have the property $a_{jk^\star} = a_2$. To make the analysis cleaner, we rename the phase variables so that $\psi_j^{(p)}$ is the phase of the jth junction in group p and $j \in [1, n_p]$. With this notation Eq. (21) becomes

$$\dot{\psi}_j^{(p)} = 1 + Ka_p \left\{ a_1 \sum_{i=1}^{n_1} \sin(\psi_i^{(1)} - \psi_j^{(p)} + \theta) + a_2 \sum_{i=1}^{n_2} \sin(\psi_i^{(2)} - \psi_j^{(p)} + \theta) \right\}. \tag{26}$$

Though various solutions exist, we are interested in those that are phase locked and exhibit maximal coherence. To this end, we search for solutions in which the junctions within each group are inphase and junctions between groups have a constant phase difference $\delta = \psi_j^{(1)} - \psi_i^{(2)}$. It is easy to show that, if such a solution exists, then

$$\delta = \sin^{-1}\left[\frac{n_1 a_1^2 - n_2 a_2^2}{a_1 a_2 K'} \sin\theta\right] - \Phi,$$

where

$$K' \cos\Phi = N\cos\theta \quad \text{and} \quad K' \sin\Phi = (n_1 - n_2)\sin\theta.$$

Note that there are phase-locked solutions if and only if

$$\left|\frac{n_1 a_1^2 - n_2 a_2^2}{a_1 a_2 K'} \sin\theta\right| \leq 1 \tag{27}$$

or, in terms of the original parameters,

$$\left|\frac{2\alpha\omega(n_1^2 a_1^4 - n_2^2 a_2^4)}{a_1 a_2 \sqrt{N^2(\omega_{k^\star}^2 - \omega^2)^2 + 4\alpha^2\omega^2(n_1 - n_2)^2(n_1 a_1^2 + n_2 a_2^2)^2}}\right| \leq 1. \tag{28}$$

With the knowledge that phase-locked solutions exist and an explicit expression for the phase difference between the two groups, we can now examine the stability of such solutions. We let $\psi_i^{(1)} = \psi_0^{(1)} + x_i$ and $\psi_i^{(2)} = \psi_0^{(2)} + y_i$, where both x_i and y_i are small. Then, to first order, Eq. (26) becomes

$$\dot{x}_j = K a_1^2 \cos\theta \sum_{i=1}^{n_1}(x_i - x_j) + K a_1 a_2 \cos(-\delta + \theta) \sum_{i=1}^{n_2}(y_i - x_j),$$
$$\dot{y}_j = K a_1 a_2 \cos(\delta + \theta) \sum_{i=1}^{n_1}(x_i - y_j) + K a_2^2 \cos\theta \sum_{i=1}^{n_2}(y_i - y_j).$$

This system is diagonalized by the coordinate transformations

$$\Gamma = \cos(\delta + \theta) \sum_{i=1}^{n_1} x_i + \cos(-\delta + \theta) \sum_{i=1}^{n_2} y_i, \qquad \Lambda = n_2 \sum_{i=1}^{n_1} x_i - n_1 \sum_{i=1}^{n_2} y_i,$$
$$\delta_i^{(x)} = x_{i+1} - x_i, \quad i = 1, \ldots, n_1 - 1,$$
$$\delta_i^{(y)} = y_{i+1} - y_i, \qquad i = 1, \ldots, n_2 - 1$$

giving

$$\dot{\Gamma} = 0, \tag{29}$$

$$\dot{\Lambda} = -K a_1 a_2 [n_2 \cos(-\delta + \theta) + n_1 \cos(\delta + \theta)]\Lambda, \tag{30}$$

$$\dot{\delta}_i^{(x)} = -K a_1 [n_1 a_1 \cos\theta + n_2 a_2 \cos(-\delta + \theta)]\delta_i^{(x)}, \tag{31}$$

$$\dot{\delta}_i^{(y)} = -K a_2 [n_1 a_1 \cos(\delta + \theta) + n_2 a_2 \cos\theta)]\delta_i^{(y)}. \tag{32}$$

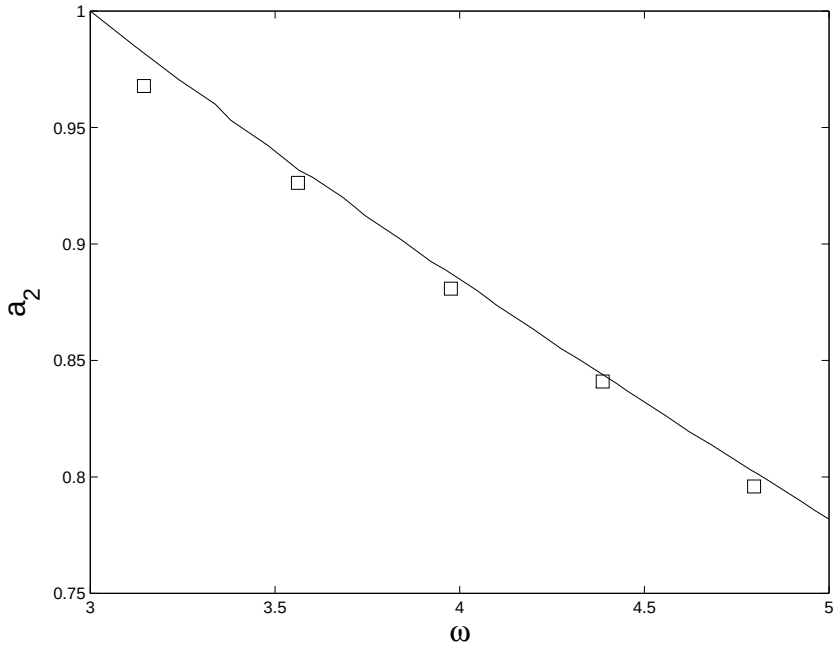

Fig. 11. Comparison of the theoretical (solid line) and numerical (squares) values of the critical value of a_2. In this example there are four junctions with $a_1 = 1$ and four junctions with variable a_2. Plotted are the theoretical and numerical values of a_2 above which phase locking becomes possible.

Fig. 11 shows a typical example of the accuracy of Eq. (28). With $\alpha = 1$, $\omega_{k^\star} = 3$, $n_1 = n_2 = 4$ and $a_1 = 1$ we plot the critical value of a_2 above which phase locking becomes possible. If a_2 is smaller than the critical value then phase locked solutions will not exist. If, however, a_2 is larger than some critical value a_{2c}, then the phase locked solution will be stable for $\omega > \omega_{k^\star}$. The solid line is the theoretical value of a_{2c} obtained from Eq. (28) while the squares are the numerical values obtained from direct integration of Eqs. (5) and (6) keeping *only* the resonant mode.

We can also check the accuracy of condition Eq. (28) in the case of the full transmission line problem (i.e., keeping all of the modes). This is somewhat trickier to do since one must be careful that the configuration chosen actually has a resonant structure. For instance, one cannot simply choose $\omega \approx \omega_{k^\star}$ and expect the $k^\star$th mode to dominate. One must also be sure that the placement of the junctions is favorable to the excitement of the chosen mode. Fig. 12 shows an example of the accuracy of Eq. (28) with such a configuration. Here there are nine junctions being driven just above the fifth mode frequency with $\alpha = 0.01$ and $v = 1/\pi$. The nine junctions are placed in three clusters of three junctions each, centered on alternating antinodes of the fifth mode (specifically, $x_j \in \{0.1, 0.1 \pm \delta x, 0.5, 0.5 \pm \delta x, 0.9, 0.9 \pm \delta x\}$). If δx is small enough, phase-locked solutions will exist and will be stable when $\omega > \omega_5$. If, on the other hand, δx is greater than some critical value δx_c, phase locking will become impossible. Plotted are the theoretical (solid line) and numerical (squares) values of δx_c. The theoretical curve was computed using Eq. (28) with $n_1 = 3$, $n_2 = 6$, $a_1 = 1$, and $a_2 = \sin((5/2)\pi(1 - \delta x))$. Meanwhile, each of the six open squares were determined from a sequence of runs with varying δx and ω held fixed. Random initial conditions were chosen for each run. The transition values were determined to within a tolerance of 10^{-3}.

The agreement is good enough that we can trust conditions (27) and (28) and we now turn to see what physical insight we can glean from them plus the stability analysis Eqs. (29)–(32). In particular, we want to know how to achieve stable locking by manipulating the placement of the junctions within the two groups.

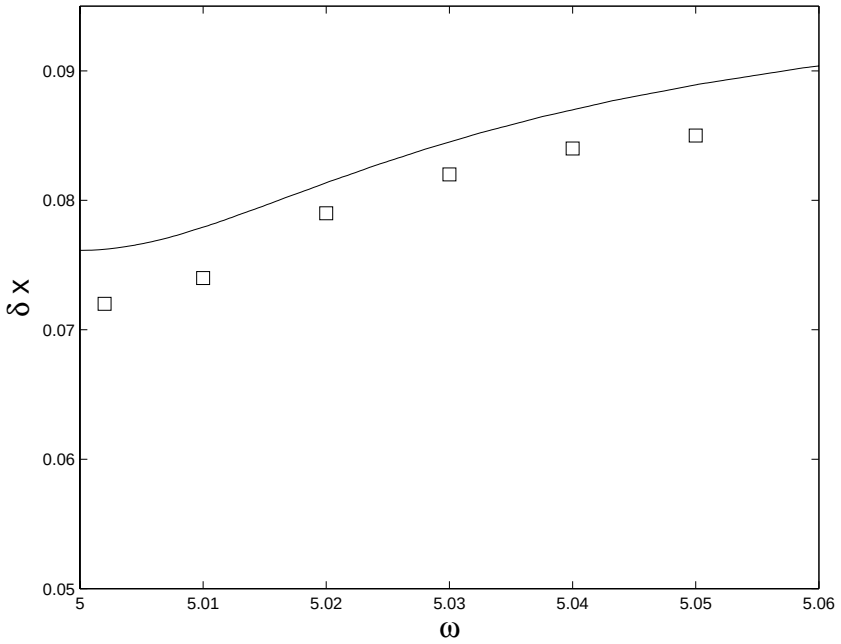

Fig. 12. Comparison of the theoretical (solid line) and numerical (squares) values of the critical value of δx. Here there are nine junctions placed at $x_j \in \{0.1, 0.1 \pm \delta x, 0.5, 0.5 \pm \delta x, 0.9, 0.9 \pm \delta x\}$, $\alpha = 0.01$, $v = 1/\pi$, and $k_{\max} = 10$. Phase locked solutions are stable below the curve.

First, it is apparent from Eq. (28) that the closer the groups are in both number and placement (with respect to the resonant mode), the better are the chances of locking. This follows from the fact that as $n_1 \to n_2$ and $a_1 \to a_2$, the numerator in Eq. (28) vanishes. This may not be the only way to create phase-locked solutions, but it does have a physical appeal that mirrors experimental attempts to create high power arrays. Han et al. [11] proposed that arrays with clusters of junctions separated by whole wavelengths near the antinodes of the resonant mode should exhibit better phase locking properties than other configurations. Eq. (28) can then tell us something about how large these clusters can be before phase locking becomes impossible.

Second, Eq. (28) also implies that the closer the system is to resonance, the *harder* it is to achieve phase locking. This becomes easier to see if one considers the case where $n_1 = n_2$. Then Eq. (28) becomes

$$\left| \frac{\alpha\omega N(a_1^4 - a_2^4)}{2a_1a_2(\omega_{k^\star}^2 - \omega^2)} \right| \leq 1. \tag{33}$$

The resonant denominator is now clearly seen in Eq. (33). Note, also, that the total number of junctions affects the stability, but in a surprising way: the higher N, the lower the chance of locking.

We can get a physical understanding of these conclusions, as follows. Consider the resonant mode as it is being driven by the junctions. The amplitude response of the mode is directly proportional to the number of junctions driving it, and inversely proportional to the difference in the squares of the frequencies. Next consider the junctions as they are being driven by the mode. Eq. (5) tells us that near resonance each junction is driven by both the dc component (I_b) and a scaled oscillatory part ($a_{ik^\star} A_{k^\star}(t)$). The difference in the driving for the two groups is then given by $(a_1 - a_2) A_{k^\star}(t)$. For phase locking to occur the amplitude of the driving difference cannot be too large. Therefore, the larger the amplitude of the mode the smaller the chance of phase locking. This is also the reason that tightly clustering the junctions increases the chance of phase locking: as $a_1 \to a_2$ the amplitude of the driving difference goes to zero.

Another configuration inspired by experiment [11,12] that falls within the two "group" case consists of one junction placed at every antinode of the resonant mode (so that they are separated by one half of a wavelength).

First consider the case where $n_1 = n_2 = 1$ and $a_1 = -a_2 = 1$. An inphase solution exists for this configuration and is stable for $\omega < \omega_{k^\star}$. This is the exact opposite of the stability condition found in the one group case and is due to the polarity reversal between the coupling constants of the two junctions.

A more complicated situation occurs when $n_1 = n_2 > 1$ and $a_1 = -a_2 = 1$. Eq. (28) implies that a phase locked solution still exists, but from Eqs. (29)–(32) one sees there are $N - 1$ zero eigenvalues and just a single non-zero eigenvalue. Numerically we have found that phase locked solutions do indeed exist for $\omega < \omega_{k^\star}$ but the value of the phase difference between the two groups (δ) can take on multiple values. This is reminiscent of the situation in the lumped circuit problem, where incoherent periodic solutions appear not individually but rather in continuous families [27,28]; more generally such indeterminacy of relative phase between locked groups is typical of clustering behavior in lumped arrays [29].

6. Summary

At sufficiently high frequencies, the wire connecting the elements of any electronic oscillator array becomes an essential dynamical entity. But for Josephson arrays especially, this new wrinkle is an important consideration. The twin technological pressures of higher powers and higher frequencies inevitably push the design of the arrays out of the lumped-circuit limit. At the same time, new experimental strategies become available through manipulation of the spatial distribution of the junctions.

In this paper, we considered perhaps the simplest non-trivial distributed architecture. The averaging scheme that we used led us to a set of equations structurally similar to those of a loaded lumped array with external load. These equations are valid for any spatial arrangement of the junctions, and thus serve as a natural springboard for investigations that compare and contrast various spatial distribution schemes. Unfortunately, the coupling constants in the averaged equations are pair dependent, and this is a major hurdle for further analysis. Nevertheless, we were able to make good progress for certain judiciously chosen examples.

In the case of near-resonant architectures we made a further reduction of the problem. The resonant case is especially revealing, and leads to significant physical insight into achieving attracting synchronized dynamics. The tighter the clusters, the more likely it is that phase locked solutions appear. Surprisingly, however, increasing the number of junctions within a cluster can hurt. The interplay between these two—which are the most fundamental properties of distributed architectures used in past experiments—is captured by the two-group model.

Further development of the theory of transmission line coupled arrays may have a broader significance than the problem we treated. For example, new schemes for power combining in nonlinear antenna arrays rely on transmission line coupling of semiconductor oscillators, as do related methods for beam scanning and beam shaping [30–32]. There are also hints that distributed arrays exhibit fundamentally different phenomena than their lumped counterparts. In one case, experiments on distributed Josephson arrays reported evidence of super-radiance [33] incompatible with any lumped description. In another, numerical simulations of both Josephson and van der Pol distributed arrays have found a novel spontaneous dimerization [34] wherein pairs of oscillators quickly synchronize but thereafter remain dynamically inert.

Acknowledgements

We thank Mukesh Dhamala and Denis Tsygankov for stimulating discussions. This work was supported by the Office of Naval Research under contract number N00014-99-1-0592.

Appendix A. Solving for the mode coefficients

When solving for the mode coefficients M_k and N_k, we are led to the linear system Eqs. (13) and (14). To solve it, we first introduce an integer cut-off parameter $k_{\max}$. In practice, $k_{\max}$ should be large, but not so large that the actual physical size of the junctions is comparable to the wavelength $2\pi/k_{\max}$ of the cutoff mode. (Recall that the transmission line model Eq. (4) treats the junctions as spatially point-like.) With this truncation the system (13) and (14) can be written as

$$\begin{pmatrix} \mathbf{a} & -\boldsymbol{\eta} \\ \boldsymbol{\eta} & \mathbf{a} \end{pmatrix} \begin{pmatrix} \vec{M} \\ \vec{N} \end{pmatrix} = \begin{pmatrix} \vec{f} \\ \vec{g} \end{pmatrix}, \tag{A.1}$$

where the matrix $\boldsymbol{\eta}$ is defined in Eq. (15), $a_{kl} = (\omega_k^2 - \omega^2)\delta_{kl}$, and the vectors $\vec{M}$, $\vec{N}$, $\vec{f}$, and $\vec{g}$ are the $k_{\max}$-dimensional column vectors defined above.

The linear system (A.1) allows us to solve for M_k and N_k (numerically, in the general case). These, in turn, give us the solutions for the A_k's such that (cf. Eq. (12)):

$$A_k = \sum_{j=1}^{N} \{[P_{jk}\cos\gamma_j + Q_{jk}\sin\gamma_j]\sin t + [R_{jk}\cos\gamma_j + S_{jk}\sin\gamma_j]\cos t\}, \tag{A.2}$$

where

$$P_{jk} = -2\alpha B^{(1)} \sum_{l=1}^{k_{\max}} a_{jl} T_{kl}, \qquad Q_{jk} = -2\alpha B^{(1)} \sum_{l=k_{\max}+1}^{2k_{\max}} a_{jl} T_{kl},$$

$$R_{jk} = -2\alpha B^{(1)} \sum_{l=1}^{k_{\max}} a_{jl} T_{(k+k_{\max})l}, \qquad S_{jk} = -2\alpha B^{(1)} \sum_{l=k_{\max}+1}^{2k_{\max}} a_{jl} T_{(k+k_{\max})l},$$

and

$$\mathbf{T} = \begin{pmatrix} \mathbf{a} & -\boldsymbol{\eta} \\ \boldsymbol{\eta} & \mathbf{a} \end{pmatrix}^{-1} \tag{A.4}$$

is the $2k_{\max} \times 2k_{\max}$ solution matrix to system (A.1).

It is evident from Eq. (A.4) that the matrix $\mathbf{T}$ will have the same block form as its inverse. This tells us that $P_{jk} = S_{jk}$ and $Q_{jk} = -R_{jk}$, allowing us to reduce Eq. (A.2) to Eq. (16).

References

[1] T.D. Clark, Phys. Lett. A 27 (1968) 585.
[2] D.R. Tilley, Phys. Lett. A 33 (1970) 205.
[3] B.D. Josephson, Phys. Lett. 1 (1962) 251.
[4] K.A. Delin, T.P. Orlando, Foundations of Applied Superconductivity, Addison-Wesley, USA, 1991.
[5] T. van Duzer, C.W. Turner, Principles of Superconductive Devices and Circuits, Elsevier, New York, 1981.
[6] P. Hadley, Dynamics of Josephson junction arrays, Ph.D. Dissertation, Stanford University, 1989.
[7] P. Hadley, M.R. Beasley, Appl. Phys. Lett. 50 (1987) 621.
[8] S. Strogatz, I. Stewart, Sci. Am. 269 (1992) 102.
[9] K. Wiesenfeld, in: M. Golubitsky, D. Luss, S.H. Strogatz (Eds.), Pattern Formation in Continuous and Coupled Systems, Springer, New York, 1999.
[10] S. Strogatz, Sync, Hyperion, New York, 2003.

[11] S. Han, B. Bi, W. Zhang, J.E. Lukens, Appl. Phys. Lett. 64 (1994) 1424.
[12] B. Bi, S. Han, J.E. Lukens, K. Wan, IEEE Trans. Appl. Supercond. 3 (1993) 2303.
[13] P.A.A. Booi, S.P. Benz, Appl. Phys. Lett. 68 (1996) 3799.
[14] A.B. Cawthorne, P. Barbara, S.V. Shitov, C.J. Lobb, K. Wiesenfeld, A. Zangwill, Phys. Rev. B 60 (1999) 7575.
[15] D. Tsygankov, K. Wiesenfeld, Phys. Rev. E 66 (2002) 036215/1–9.
[16] J.W. Swift, S.H. Strogatz, K. Wiesenfeld, Physica D 55 (1992) 239.
[17] S. Watanabe, S.H. Strogatz, Physica D 74 (1994) 197.
[18] K. Wiesenfeld, P. Collet, S.H. Strogatz, Phys. Rev. Lett. 76 (1996) 404;
Phys. Rev. E 57 (1998) 1563.
[19] A.K. Jain, K.K. Likharev, J.E. Lukens, J.E. Sauvageau, Phys. Rep. 109 (1984) 309.
[20] K. Wan, A.K. Jain, J.E. Lukens, Appl. Phys. Lett. 54 (1989) 1805.
[21] B. Vasilić, S.V. Shitov, C.J. Lobb, P. Barbara, Appl. Phys. Lett. 78 (2001) 1137.
[22] G.A. Ovsyannikov, Z.G. Ivanov, J. Mygind, N.F. Pederson, Physica B 194–196 (1994) 107.
[23] M. Dhamala, K. Wiesenfeld, Phys. Lett. A 292 (2002) 269.
[24] K.K. Likharev, Dynamics of Josephson Junctions and Circuits, Gordon and Breach, New York, 1986.
[25] J.E. Savageau, Phase-locking in distributed arrays of Josephson junctions, Ph.D. Dissertation, State University of New York, Stony Brook, 1987.
[26] K. Wiesenfeld, J.W. Swift, Phys. Rev. E 51 (1995) 1020.
[27] S. Nichols, K. Wiesenfeld, Phys. Rev. A 45 (1992) 8430.
[28] S. Watanabe, S. Strogatz, Physica D 74 (1994) 194.
[29] I.B. Schwartz, K.Y. Tsang, Phys. Rev. Lett. 73 (1994) 2797.
[30] R. York, Z. Popovic (Eds.), Active and Quasi-optical Arrays for Solid State Power Combining, Wiley, New York, 1997.
[31] R. Pogorzelski, IEEE Microwave Guided Wave Lett. 10 (2000) 478–480.
[32] T. Heath, Synchronization and phase dynamics of coupled oscillators, Ph.D. Dissertation, Georgia Institute of Technology, 1999.
[33] P. Barbara, A. Cawthorne, S. Shitov, C. Lobb, Phys. Rev. Lett. 82 (1999) 1963.
[34] D. Tsygankov, K. Wiesenfeld, Spontaneous Formation of Inert Oscillator Pairs, Preprint, 2003.